Advanced injection cooling concept for Organic Rankine Cycles

Sebastian Eyerer [a], Fabian Dawo [a], Roberto Pili [a], Anne Niederdränk [a], Roland Windhager [a], Christoph Wieland [a] and Hartmut Spliethoff [a,b]

[a] Technical University of Munich, Institute for Energy Systems, Garching, Germany, sebastian.eyerer@tum.de, CA
[b] Bavarian Center for Applied Energy Research, Garching, Germany

Abstract:

The present experimental and numerical investigation is about an efficiency increasing and/or cost-reducing measure for Organic Rankine Cycle (ORC) systems. In such systems, a high proportion of the self-consumption of the system lies in the condensation of the working fluid due to the operation of ventilators or cooling pumps. Typically, the condenser heat exchanger is one component, where the processes of desuperheating, condensation and in some applications also subcooling takes place. Especially, the process of desuperheating requires huge heat exchanger surfaces due to the low heat transfer coefficients of the gas phase. The proposed measure aims in reducing the share of desuperheating in the condenser by injection cooling in front of the condenser. Thus, on the one hand, the condenser surface area can be smaller, reducing investment costs. On the other hand, if the surface area is kept constant, the expansion backpressure can be reduced due to the improved heat transfer in the condenser, leading to a higher power output of the expansion machine. The present study demonstrates the benefit of this optimization measure by an experimental investigation, which is complemented by a numerical analysis. With this measure and R1233zd-E as working fluid, the condensation pressure can be decreased by up to 11.2% leading to an increase in net power output of 7.9%. With this, quite substantial additional revenue is generated especially with a high full load operation.

Keywords:

Bubbler, Condensation, Desuperheating, Efficiency enhancement, Injection cooling.

1. Introduction

In recent years, the effects of global warming, with extreme weather events, become more and more apparent. According to the Paris Agreement of the UN framework convention on climate change, the global average temperature should be limited to below 2 °C above pre-industrial levels [1]. In order to meet this goal, considerable efforts to decrease greenhouse gas emissions are necessary. Within the energy sector, there are two main approaches to reduce these emissions. First, the energy efficiency on the demand side may be increased, to reduce the total consumption. Second, the share of renewable energy sources for power and heat production may be increased, to reduce the emissions on the production side.

In this context, the Organic Rankine Cycle (ORC) is a promising technology focusing on both approaches. The ORC enables low-temperature heat sources to be used for power generation and can thus be applied to industrial waste heat and renewable sources such as solar heat, geothermal brine or biomass combustion. Furthermore, the ORC technology is well suitable for combined heat and power production, which is often applied in geothermal projects.

Especially in large-scale application, such as geothermal, the condensation of the working fluid significantly contributes to the self-consumption of the plant. This is especially true for air-cooled condensers. Depending on the ambient conditions and the current operation point of the plant, the power consumption of an air-cooled condenser can be up to 20 % of the turbine gross power output [2]. Due to this high proportion of the systems self-consumption, the optimization of the condenser operation is promising to increase the net power output and the net system efficiency. To this end, especially optimization measures for increasing the heat transfer coefficient (HTC) on both, the cooling medium side and the ORC working fluid side has been studied in literature. For example, Li et al. [3] developed a liquid-separated condensation method, where liquid condensate is extracted from the two-phase flow during the condensation process. Typically, the HTC drops with decreasing vapor quality, since the heat exchanger surface is more and more occupied by the liquid fluid. Thus, the separation of this liquid condensate leads to an increased HTC along the flow path. Another study concerning the optimization of the condensation process has been made by Usman et al. [4]. They compared an air-cooled and a wet cooling tower based ORC in part-load operation. They reported a significantly lower overall heat transfer in the case of the air-cooled condenser, leading to higher surface areas and thus almost double investment costs compared to the wet cooling tower.

In this study, another measure will be presented to optimize the HTC in the condenser. Since the ORC working fluids often have a positive or zero slope of the dew curve, the state after expansion is highly superheated vapor. In the condenser the processes of desuperheating, condensation and in some applications also subcooling then take place. Especially, the process of desuperheating requires huge heat exchanger surfaces due to the low HTC of the gas phase. Thus, proposed measure aims in reducing the share of desuperheating in the condenser due to injection cooling in front of the condenser. This measures has been patented by some of the authors [5]. The purpose of this study is thus, to investigate this injection cooling measure within an ORC test rig and numerical simulations and to prove its performance.

In order to meet this purpose, the system layout and basic functionality will be described first. Then, the ORC test rig and the methodology of the experiments will be explained. In section 4, the modelling approach will be introduced and the model will be validated. The experimental and simulative results will then be presented and discussed in section 5 and relevant conclusions are drawn in section 6.

2. System description and basic functionality

In this section, the system architecture will be introduced and the functionality of the injection cooling will be explained.

The standard ORC layout is depicted in Fig. 1(a). It consists of a preheater (a), an evaporator (b), an expander (d), a condenser (c) and a feed pump (e). For injection cooling, a further line with cold liquid working fluid is needed. Two variants of this line are indicated in Figs 1(b) and 1(c) with the blue lines. The cold liquid fluid can either be extracted in the high-pressure line after the feed pump (cf. Fig. 1(b)). The injection flow rate can then be controlled with a valve in the injection line. In the other variant, the cold liquid fluid is extracted directly after the condenser in the condensate line (cf. Fig. 1(c)). In that case, an injection pump is required to lift the condensate pressure above the pressure of the exhaust vapor. Again, the injection flow rate can be controlled via the valve in the injection line. In both variants, the cold liquid working fluid will be injected into the superheated exhaust vapor. There, the cold liquid fluid cools down the exhaust vapor and thereby evaporates. Depending on the injected flow rate, the superheating at the condenser inlet can be reduced. The maximum reasonable injection flow is the one, where saturated vapor enters the condenser.

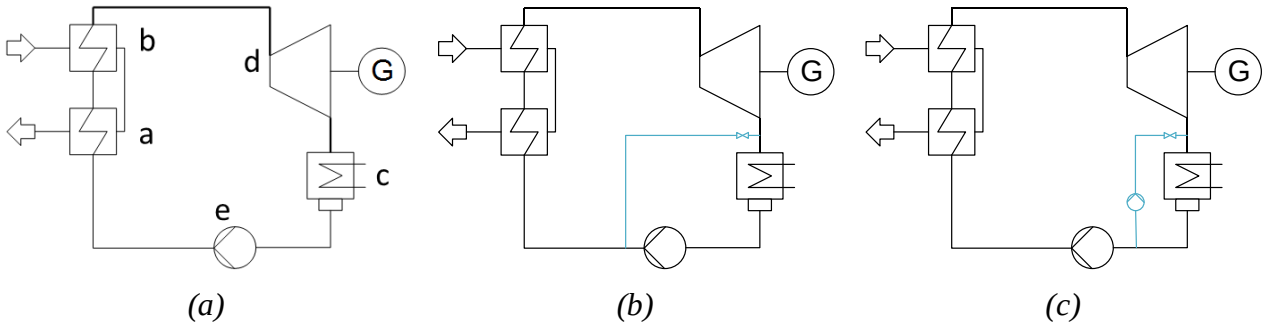

Figure 1. System layout: a) standard ORC, b) variant 1 of the injection cooling, c) variant 2 of the injection cooling.

The basic functionality of the injection cooling is explained in Fig. 2. Figure 2(a) shows a schematic sketch of the heat transfer processes in a condenser of a standard ORC. Since the heat transfer coefficients are quite low within the gas phase, a large proportion of the heat exchanger surface is needed for desuperheating. According to García del Valle et al. [6], the HTC during desuperheating of R134A is typically in the range of 0.2-0.5 kW/m^{2}K. In contrast, the condensation HTC of R134A is typically in the range of 0.7-2.5 kW/m^{2}K [6]. Kwon et al. [7] reported the same typical range of the condensation HTC of R1233zd-E. With the injection cooling, the superheating is done by mixing with the liquid fluid as indicated in Fig. 2(b). Depending on the injected flow rate, a much smaller or even no surface area is needed in the condenser. Due to the higher HTC during phase-change, the overall HTC within the condenser can be increased with the proposed measure. However, due to the higher flow rate through the condenser, the pressure drop over this component might increase, which would be negative in terms of the expander pressure ratio. The influence of both contrary effects, higher HTC and possible higher pressure drop, will be discussed in section 5.

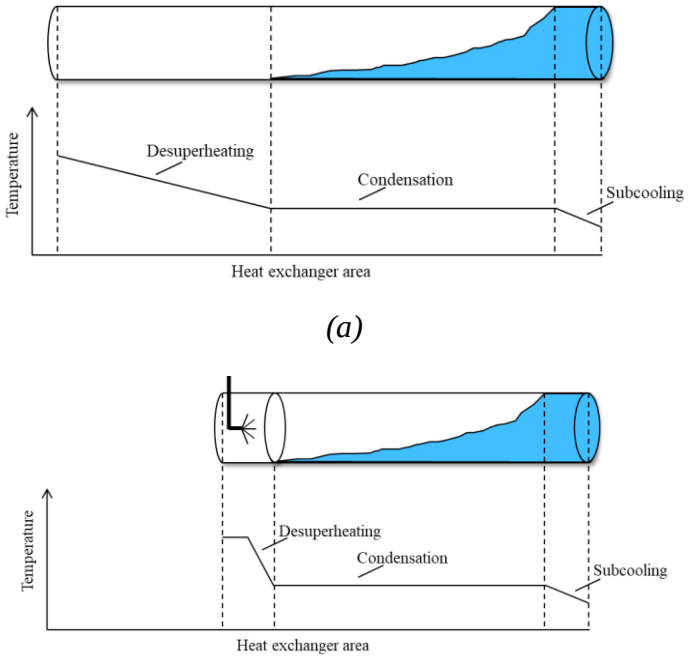

Figure 2. Schematic sketch of the heat transfer processes in a horizontal condenser tube: a) standard ORC without injection cooling, b) injection cooling.

The increased HTC, due to the injection cooling can now be utilized in two different ways. In the case of a new build ORC system, the condenser heat exchanger area may be reduced, which will

reduce the investment cost and the footprint of the component. In the case of existing plants, the injection cooling can be implemented as a retrofit measure. The increased HTC within the condenser may cause lower condensation temperatures leading to a larger pressure ratio over the expansion machine and thus higher power outputs.

3. Experimental facility and methodology

In order to demonstrate the injection cooling, the above-described variant 1 (cf. Fig. 1(b)) has been implemented in an ORC test rig. The experimental setup with all options for controlling the process parameters is described in this section. Furthermore, the applied measurement devices as well as their accuracies are specified. Finally, the experimental procedure is presented and the data post processing is described.

3.1. ORC system and control options

In Fig. 3, a simplified P&I diagram of the ORC test rig and the heat source with every relevant measuring point is shown. The heat source of the ORC consists of an electrical resistance heater with 200 kW electrical power and a hot water circuit. The mass flow in the hot water circuit is controlled by means of the rotational speed of the centrifugal pump. Pulse width modulation of the electrical heater allows controlling the temperature of the heat source at the heat exchanger inlet. The evaporator is a brazed plate heat exchanger from Alfa Laval (CBH112-52H-F). It transfers the heat to the ORC system while preheating, evaporating and superheating the working fluid. The working fluid for the measurement campaign of this work is R1233zd(E), which is a low-GWP alternative to R245fa [8]. After the heat exchanger, the fluid enters the expander. This test rig utilizes an open drive twin-screw compressor from Bitzer (OSN5361-K) in reverse mode as an expansion machine. The built-in volume ratio is 3.1 with a swept volume of 0.678 l on the low-pressure side. A frequency converter allows controlling the rotational speed of the generator shaft, which is directly coupled to the twin-screw expander. The produced electrical power is measured and fed to the grid. By adjusting the rotational speed of the expander, the live vapor pressure of the ORC can be controlled.

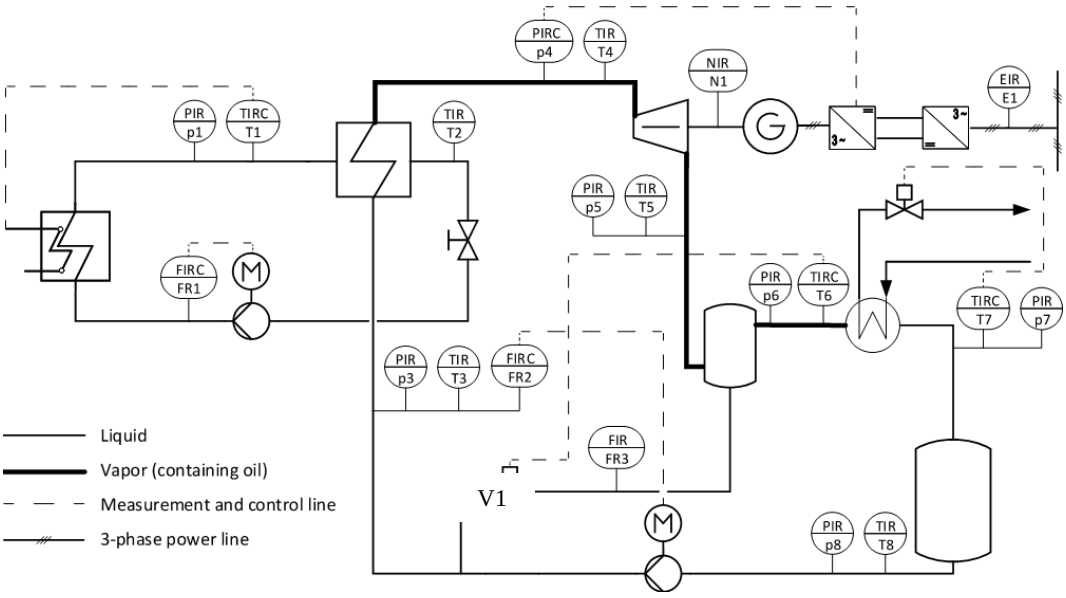

Figure 3. Simplified P&I diagram of the ORC test rig.

The expanded exhaust vapor leaves the expander and enters a 30 l bubbler tank, where the superheated vapor is mixed with cold pressurized fluid. Figure 4(a) shows a sectional drawing of the pressure vessel with all internals. The exhaust vapor enters the bubbler through the flange on the right-hand side (cf. Fig. 4(b)). Then it is guided into the vessel volume via a closed pipe with small drilled holes. This ensures that the vapor is evenly distributed throughout the entire volume and is well mixed with the liquid. A trunk-shaped tube at the rear of the tank directs the cold liquid to the bottom of the

container, which then mixes with the superheated vapor. The volume flow of the recirculated cold liquid is measured and an electric control valve, which adjusts the liquid volume flow, can control the degree of superheating after the tank. The cooled vapor leaves the tank through the connecting flange on the left-hand side and enters the condenser, which is a brazed plate heat exchanger from Alfa Laval (CB112-170H). Next, the condensate flows into a buffer tank and is then pressurized to the live vapor pressure by a piston diaphragm pump. The rotational speed of the pump is controlled to adjust the mass flow rate through the evaporator, to the desired value.

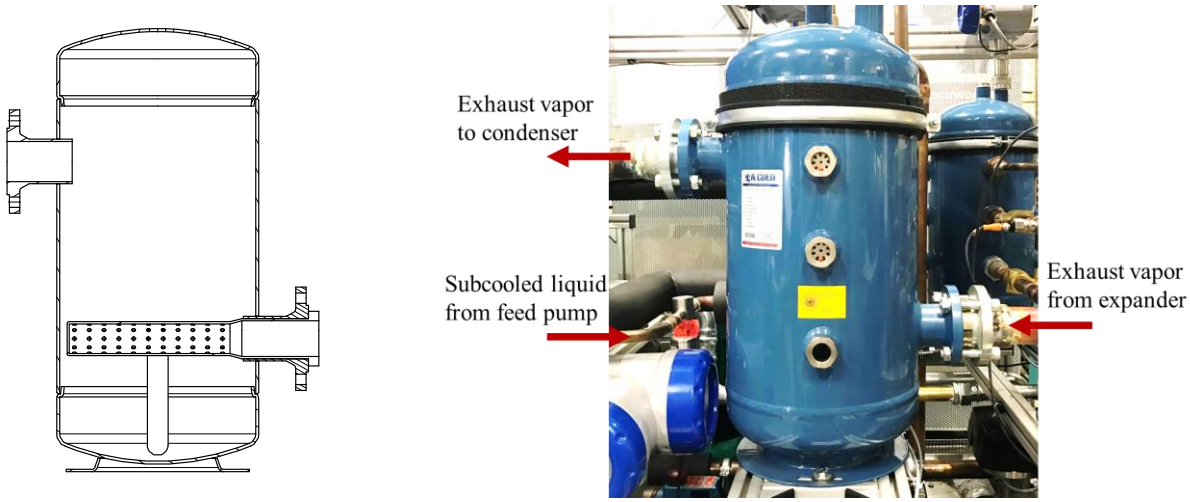

(a) *(b)*

Figure 4. Bubbler tank: a) Sectional drawing with internals, b) photo of the tank.

As indicated in Fig. 3., the ORC system is fully instrumented, having temperature and pressure sensors before and behind each component, measuring the total and the injected mass-flow rate as well as having sensors for electrical power measurement. All the instrumentation and measuring ranges as well as the accuracy of each sensor is summarized in Table 1.

Table 1. Measuring range and accuracy of the relevant sensors.

Measured parameter	Measurement principle	Measuring range	Accuracy of measurement	Sensors	Output signal
Pressure	Strain gauge	0 - 16 bar 0 - 40 bar 0 - 60 bar	±0.08 bar ±0.20 bar ±0.30 bar	p5-p8 p4 p3	4-20 mA
Temperature	PT100	-100 - 400 °C 0 0 - 150 °C	±(0.002·MV+0.15 °C) ±(0.0017·MV+0.1 °C)	T3 All other	resistance
Total mass flow rate	Coriolis sensor	0 - 1.5 kg/s	±(0.0015·MV+ 0.7502 kg/s)	FR2	4-20 mA
Inj. volume flow rate	Displacement sensor	1 - 30 l/min	±0.3 l/min	FR3	digital
El. gross power output	El. power meter	0 - 40 kW	±0.01·MV	E1	digital

In order to obtain the measurement errors, accuracy of the sensor and the data acquisition system need to be considered. Therefore, Table 2 shows the precision of the used I/O modules from National Instruments along with an allocation of the connected signals.

Table 2. Range and accuracy of the relevant I/O modules.

I/O Module	Range	Module Accuracy	Connected signals
NI 9208	-22 – 22 mA	$\pm(0.0076 \cdot I + 9.08 \cdot 10^{-3}$ mA)	Pressure sensors, Coriolis sensor
NI 9216	0 – 400 Ω	± (0.00007·I + 0.1654 °C)	All PT100
NI 9425	0 – 24 V	$\pm 3.39 \cdot 10^{-5}$ l/min [a] ± 36 W [a]	Displacement sensor Power meter

[a] Maximum discretization error

3.2. Methodology of experiments

For an objective and comprehensive evaluation of the injection cooling, in total 21 stationary operation points in full load and part load operation are investigated. For all experiments, the heat source temperature and the heat source flow rate are controlled to constant values of 135 °C and 3.5 kg/s, respectively. The same is done for the heat sink, where the temperature is controlled to 20 °C. In order to operate the ORC system in different load cases, the working fluid mass flow rate is controlled to 650 g/s (full load), 450 g/s (part load 1) and 300 g/s (part load 2). For each of these load cases, the heat sink flow rate is adjusted, such that the condensation temperature is approximately 45 °C in the case without liquid injection. Starting with a completely closed injection valve V1 (cf. Fig. 3), it has been opened stepwise, to increase the injected flow rate. The maximum valve position is the one, where saturated vapor enters the condenser. This stepwise opening of the injection valve V1 has been done separately for each of the three load cases. With this approach, the influence of the injected flow rate can be investigated and the effect of injection cooling can be compared with a standard ORC with a conventional condenser. For all operating points, stationary conditions are maintained for at least 10 min. For data evaluation, a measurement value is acquired for each sensor every second. In order to post process these raw data, an algorithm has been developed to detect the best stationary points. This algorithm is described in more detail in the next section.

3.3. Data post processing

Before the experimental data can be used appropriately for evaluation, it is post processed by an algorithm. At first, the experimental results are divided into stationary sections by identifying the specific times at which a change in the key control variable occurs. In this case, the substantial control variable is the position of the injection valve V1. After the stationary sections have been found, intervals of four minutes (240 measurements) with the lowest deviation are determined. Therefore, the normalized mean absolute error $NMAE_i$ is calculated by equation (1) for the most important variables i for each interval of four minutes within a stationary section. These variables include the live vapor pressure and temperature, condenser inlet pressure and temperature, as well as the rotational speed of the expander and the electrical power of generator. Moreover, the injection mass flow and mass flow through the expander are considered as well.

$$NMAE_i = \frac{\frac{1}{n}\sum_{t=1}^{n}\left|\bar{Y}_i - Y_{t,i}\right|}{\bar{Y}_i} \tag{1}$$

Here, $Y_{t,i}$ represents the measured value at a point of time t, while $\bar{Y}_i$ represents the average of the 240 measurements. In order to be able to compare the deviations of the different intervals, a total error is determined for each interval by summing up the individual normalized mean absolute errors $NMAE_i$. The section with the lowest error will then be averaged to represent the corresponding steady state for further analysis. Using these steady state operation conditions, further relevant properties such as enthalpy, entropy and density are calculated with Refprop 10.0 [9]. The measured values, together with the calculated fluid properties, are used to obtain characteristic process parameters. Based on the accuracies of the sensors and the data acquisition system (cf. Tables 1 and 2), the measurement errors of each value is calculated using the Gaussian law of error propagation.

4. Simulation and validation of the model

A numerical model of the condenser has been developed in the Modelica-based software Dymola, by using the commercial library TIL. The software can simulate the dynamic behavior of the condenser, but only the steady-state results will be considered in the following. The condenser model is shown in Fig. 5. The plate heat exchanger is discretized in 15 cells (based on the authors' experience) over the height of the heat exchanger, following a finite volume approach. Analogously to the experiments, R1233zd(E) is used as working fluid and the heat exchanger is modeled in counter-current operation, while its outlet is connected to a condensate receiver. With this, saturated liquid leaves the condenser.

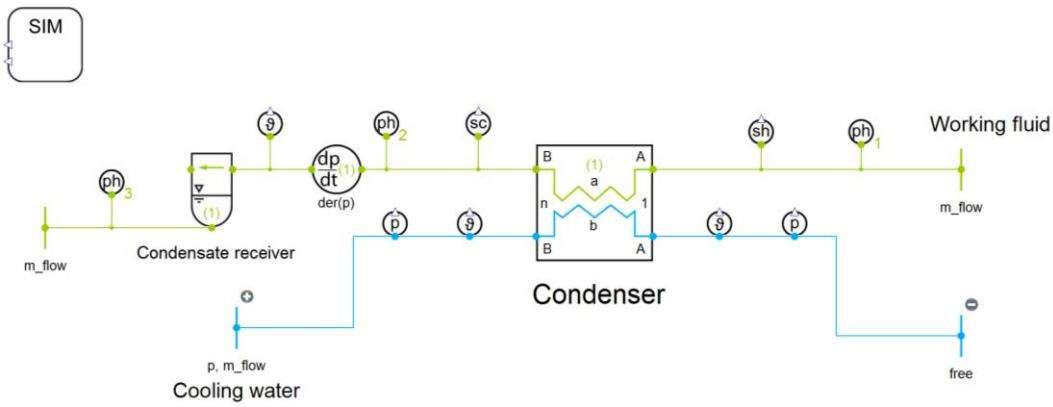

Figure 5. Model set-up for numerical simulations in Dymola.

The input geometry of the heat exchanger is detailed in Table 3. Furthermore, the same boundary conditions as in the experiments are used as input parameters. For the cooling water, the inlet temperature, pressure and mass flow rate are given, whereas only the inlet temperature and the mass flow rate are set for the working fluid. This allows the pressure to be determined by the condensing conditions in the heat exchanger, in line with the physical processes occurring in the real set-up. In order to achieve the best possible agreement between the model and the experimental data, the chevron angle, the plate thickness as well as the plate distance has been adjusted. The finally obtained values are summarized in Table 3. The correlations used to determine the heat transfer coefficient and the pressure drop of both fluids are given in Table 4.

Table 3. Geometry of the condenser.

Input parameter	**Plate width**	**Plate height**	**Number of plates**	**Plate material**
	191 mm	616 mm	170	Stainless Steel (Alloy 316)
Adjusted parameter	**Plate thickness**		**Chevron angle**	**Plate distance**
	0.4 mm		75° to vertical	1.6 mm

Table 4. Heat transfer and pressure drop correlation used in the Dymola model.

Fluid	**Phase**	**Heat transfer coefficient, W/m²K**	**Pressure drop, bar**
Working fluid	Liquid or vapor	VDI Heat Atlas, Ch. N6 [10]	VDI Heat Atlas, Ch. N6 [10]
	two-phase region	Yan, Lio, Lin [11]	Yan, Lio, Lin [11]
Cooling water	liquid	VDI Heat Atlas, Ch. N6 [10]	VDI Heat Atlas, Ch. N6 [10]

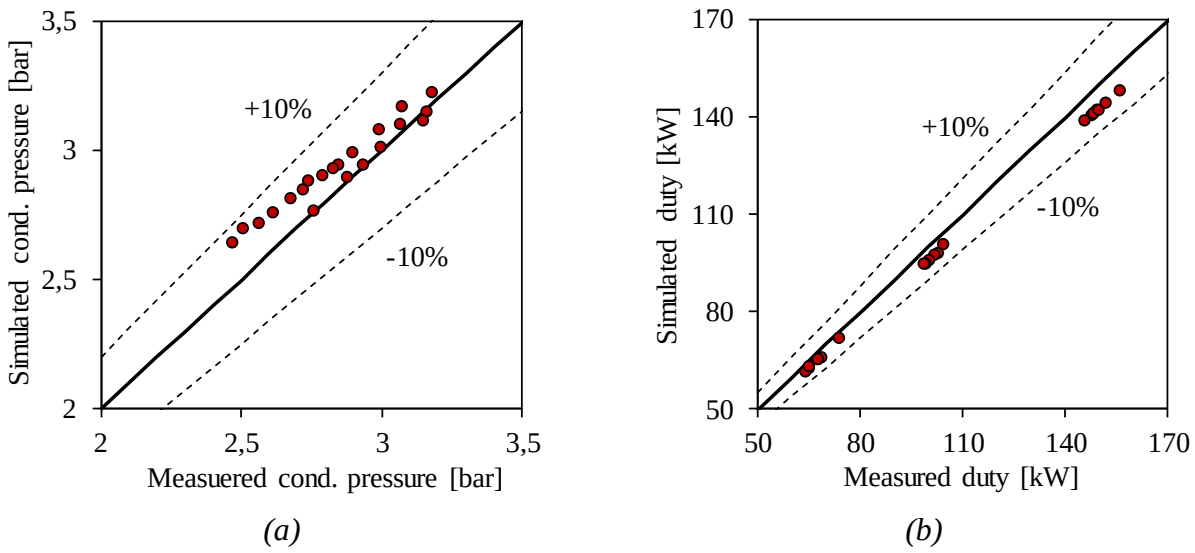

Figure 6. Model validation: a) condensation pressure, b) condenser duty.

The validation of the simulation model is done against the above-described 21 stationary operation points and is exemplarily shown in Fig. 6 for the condensation pressure and the condenser duty. These two values are chosen because they are the most relevant parameters for the injection cooling. The comparison shows that both simulated parameters are in good agreement with the experimental data, since the deviations are less than ± 10%. In Fig. 6(b), it can be seen that the model systematically underestimates the condenser duty. In the experiments, a slight subcooling of the condensate of 3-6 K has been measured. Due to the direct connection of the condenser to the buffer tank, this subcooling is not considered in the condenser model, which causes the slightly lower duty.

5. Results and discussion

With the validated simulation model and the experimental procedure described above, the injection cooling will be investigated and the effects on the heat transfer processes in the condenser will be analyzed. The influence of the injected mass-flow rate will be studied first by using the experimental data and second with the simulation model.

5.1. Experimental results

In this section, the experimental results of the injection cooling are presented. In all figures, stationary operating conditions are depicted together with the corresponding measurement errors. In order to show the impact of the injected flow rate for all three load cases better, the injection ratio Ψ_{inj} is defined as the ratio between the injected mass flow and the working fluid mass flow in the expander:

$$\Psi_{inj} = \frac{\dot{m}_{inj}}{\dot{m}_{exp}}. \tag{2}$$

With this definition, Fig. 7(a) shows the degree of superheating at the inlet port of the condenser. It can clearly be seen, that the superheating droops with increasing injection ratio. This effect can be observed for all three load cases. Thus, it can be stated, that the desuperheating can effectively be done with the injection cooling measure. Depending on the injection ratio, it is possible that the exhaust vapor enters the condenser as saturated vapor.

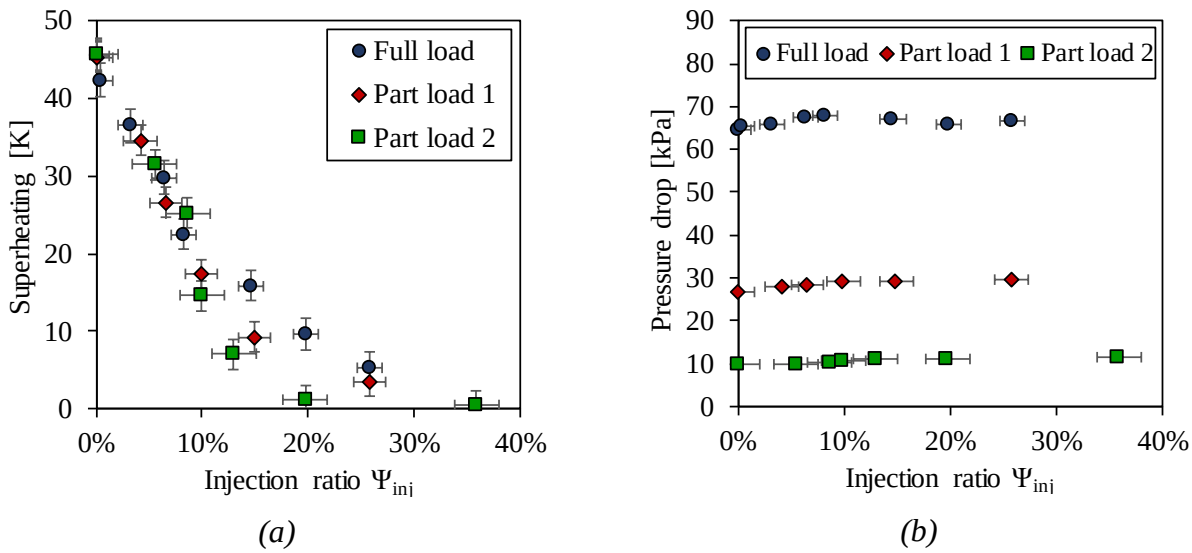

Figure 7. Influence of the injection rate: a) degree of superheating at the condenser inlet, b) pressure drop in the exhaust gas line and the condenser.

As stated above, the mass flow rate through the condenser will increase due to the liquid injection: $\dot{m}_{cond} = \dot{m}_{exp} + \dot{m}_{inj}$. Therefore, it might be possible, that the liquid injection lead to an increase in

pressure drop over the condenser, which in turn would decrease the pressure ratio over the turbine. In order to analyze this effect, the cumulated pressure drop within the exhaust vapor line and the condenser is depicted in Fig. 7(b). There, the three load cases can clearly by distinguished. Furthermore, only a very slight increase in pressure drop of less than 2 kPa can be detected, when the injection ratio is increased. This effect can be explained with two observations: On the one hand, the pressure drop within the condenser increases by up to 15 kPa due to the higher flow rate. However, on the other hand, the pressure drop in the exhaust vapor line decreases by almost the same value. This can be explained by the lower temperature and thus higher density of the exhaust vapor. Hence, the flow velocity is reduced, also reducing the pressure drop.

As described in section 2, it was expected, that the injection cooling leads to a reduction of the condensation pressure and thus to an increased power output of the expander. However, this effect could not be proven in the experiments as shown in Fig. 8(a). There, the relative change of the condensation pressure, which is defined as the average pressure between the inlet and outlet pressure, is depicted over the injection ratio. It can clearly be seen, that the condensation pressure increases, independent of the load case, by up to 17% due to the liquid injection. Since this observation is in contrast to the previous expectations, this effect will be analyzed in the following.

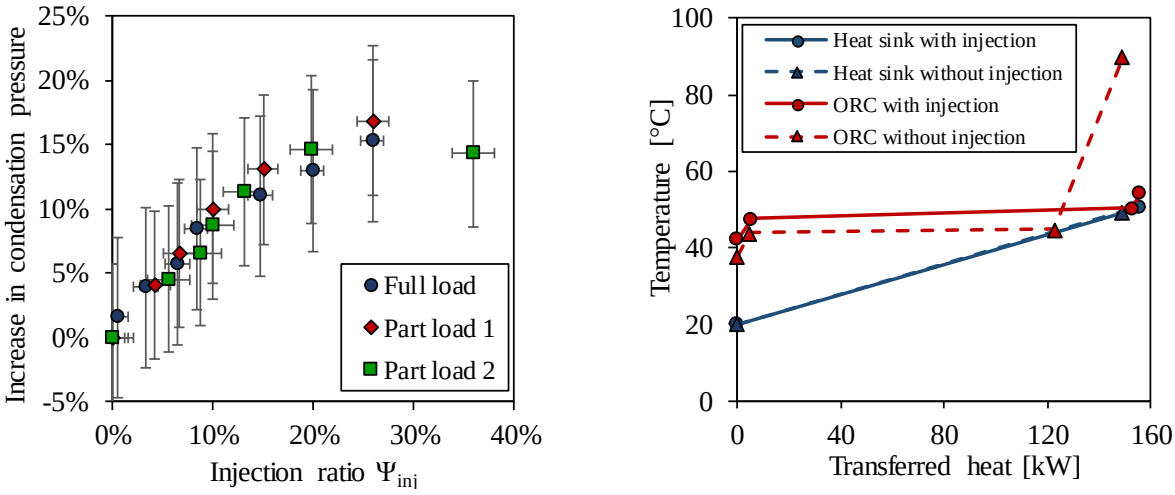

(a) *(b)*

Figure 8. Influence of the injection rate: a) condensation pressure, b) TQ-Diagram.

Figure 8(b) shows the temperature over the transferred heat for the processes in the condenser. Here, the full load operation without and maximal injection are depicted. In the case of the standard configuration without injection, approximately 18% of the total transferred heat accounts for the desuperheating process. This proportion almost vanishes in the case of the maximum injection, since the superheating is already done due to the liquid injection (cf. Fig. 7(a)). Additionally, it can be seen in Fig. 8(b) that the pinch point position of the heat transfer is at the state of saturated vapor, independent of whether the injection is active or not. When looking at the pinch point temperature difference, the reason for the increasing condensation pressure becomes obvious. In both cases, the pinch point temperature difference is below 0.5 K, which means, that the condenser surface area is highly oversized for this application. Thus, the condensation pressure is not limited by the HTC but only by the flow rate and temperature of the cooling medium. In such cases, an optimization of the HTC is not purposeful. The oversizing in the case of the present condenser is done because the ORC test rig is constructed for multiple experiments, where some requires a higher condenser duty. In real applications, the condenser would not be oversized and typical pinch point temperature differences are in the range of 5-15 K. In order to evaluate the proposed injection cooling for such real applications, the simulation results are presented in the next section.

5.2. Simulative results

In this section, the proposed injection cooling measure is analyzed with the above-described simulation model. According to the experimental results, the injection cooling is only a suitable measure, when the condensation pressure is limited by the heat transfer within the condenser. In order to investigate the case of a limiting HTC, the surface area of the condenser is reduced in the validated model. Thereby, only the plate length is downsized, in order to ensure the same hydraulic diameter and thus the same flow velocity. With this approach, the validation remains accurate. In a first step, the surface area is adjusted, such that the pinch point in full load operation without injection is increased to 15 K. For this smaller condenser, the heat transfer has now a significant limiting effect on the condensation pressure and the injection cooling measure can be investigated in conditions close to the real application. Similar to Fig. 8(a), the relative change in the condensation pressure of this smaller condenser is depicted in Fig. 9(a). Again, the average value of the inlet and outlet pressure is used for the condensation pressure. In contrast to the experimental results with the oversized condenser, a decrease in condensation pressure can be observed for a smaller heat exchanger. The condensation pressure can be reduced by up to 11.2%, which corresponds to 415 kPa. Furthermore, the decrease in pressure can be achieved for all three load cases, although the absolute reduction is higher for the full load case because of the higher condenser duty in this case. This significant reduction of the condensation pressure can be explained by the enhanced heat transfer within the condenser. In Fig. 9(b), the mean HTC on the hot side of the condenser is depicted. Due to the reduction of the share of desuperheating within the condenser, the mean HTC can be increased by up to 93.3%.

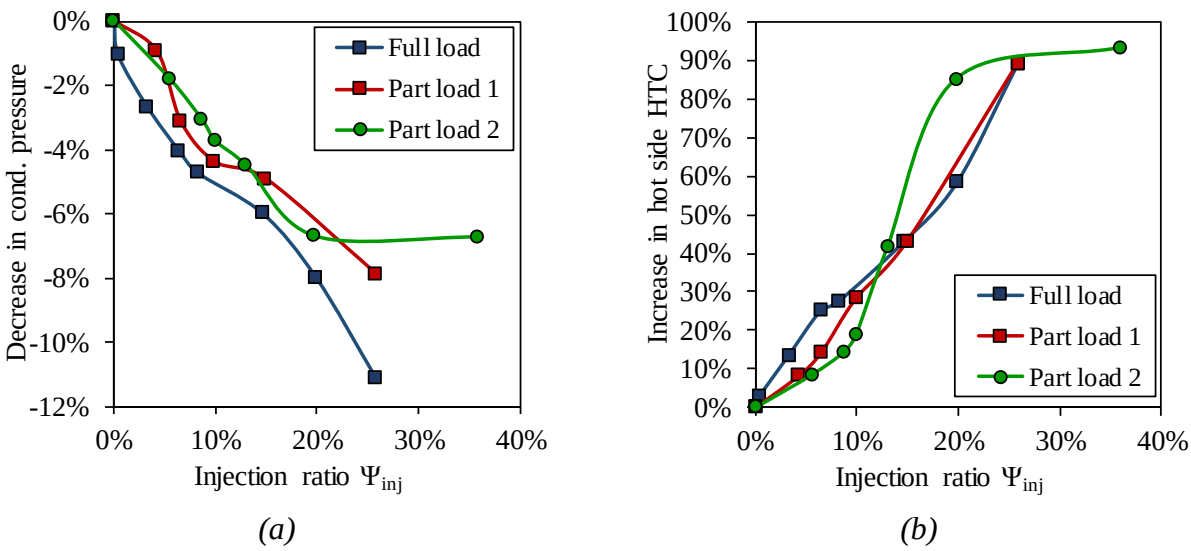

Figure 9. Influence of the injection rate with a smaller condenser: a) condensation pressure, b) mean hot side heat transfer coefficient.

The effect of the injection cooling measure is further analyzed in Fig. 10. For the full load operation, the enhanced heat transfer due to the injection cooling can decrease the pinch point temperature difference from 15 K to 7.5 K (cf. Fig. 10(a)). For this simulation, an injection ratio of 26% is used, which is the maximum injection ratio from the experiments, where the exhaust vapor enters the condenser in almost saturated state. Furthermore, it can be seen in Fig. 10(a) that the transferred heat increases due to the injection cooling. This again proves the functionality of the proposed measure.

In the case of full load operation, the reduction of the condensation pressure by 11.2 %, the pressure ratio over the expander can be increased by 12.3%. This would lead to an increase in gross power output of 8.7%. Due to the higher flow rate through the condenser and thus also through the feed pump, the net power output can be increased by only 7.9%.

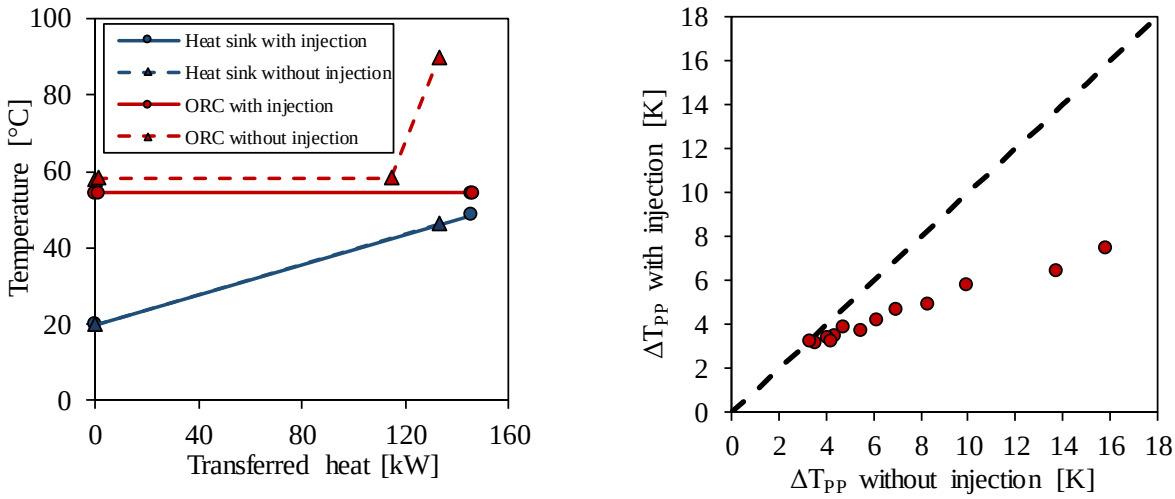

(a) *(b)*

Figure 10. Effects of the injection cooling: a) TQ-Diagram, b) Pressure reduction for difference condenser sizes.

In order to analyze the injection cooling for different heat exchanger surface areas, Fig. 10(b) compares the pinch point temperature differences in full load operation for the cases with and without injection. For this investigation, again an injection ratio of 26% is applied such that the exhaust vapor enters the condenser as saturated vapor. The figure can be read as follow: For a condenser, which is designed i.e. for a 10 K pinch point temperature difference, the injection cooling measure can reduce the temperature difference to 5,7 K. As long as the data points are below the dashed parity line, the injection cooling measure is able to reduce the pinch point temperature difference and thus also the condensation pressure. From this investigation, it can be seen, that the injection cooling measure is suitable for condensers, which have a pinch point temperature difference higher than 4 K in the conventional operation without injection cooling. This analysis is in good agreement with the experimental results, which revealed that the injection cooling has no positive effect on a condenser with a pinch point temperature difference below 0.5 K.

6. Conclusions

In this paper, the injection of liquid working fluid into the exhaust vapor line of an Organic Rankine Cycle system has been presented. This injection cooling measure has been introduced with the basic functionality and then analyzed in depth with an experimental investigation and a modelling approach. Based on that analysis, the following conclusions can be drawn:

- The desuperheating of the exhaust vapor can effectively be done with the injection cooling measure. Thus, more heat exchanger surface area is available for condensation of the fluid.
- The experiments revealed that the pressure drop in the exhaust line and the condenser does not increase due to a higher flow rate in the condenser.
- In a condenser with 15 K pinch point temperature difference, the condensation pressure can be reduced by up to 11.2% using the injection cooling.
- With this pressure reduction, the injection cooling leads to 8.7% higher gross power output and 7.9 % higher net power output of the ORC system.
- The analysis of different condenser surface areas revealed, that the injection cooling measure is suitable for condensers with a pinch point temperature difference higher than 4 K in the conventional operation without injection cooling.

Acknowledgments

Funding from the Bavarian State Ministry of Education, Science and the Arts in the framework of the project Geothermal-Alliance Bavaria is gratefully acknowledged.

Nomenclature

Letter symbols

$\dot{m}$	mass flow rate, kg/s
n	number of measurements
$NMAE$	normalized mean absolute error
p	absolute pressure, bar
$\dot{Q}$	heat flow, W
T	temperature, °C
Y	measured quantity

Greek symbols

Ψ	injection ratio

Subscripts and superscripts

exp	expander
i	index of measurement
inj	injection
t	time

References

[1] United Nations Framework Convention on Climate Change. Paris Agreement, Conference of the Parties - 21st Session (COP21); December 2015.

[2] Eyerer S, Schifflechner C, Hofbauer S, Bauer W, Wieland C, Spliethoff H. Combined heat and power form hydrothermal geothermal resources in Germany: A potential assessment. Submitted to Sustainable and Renewable Energy Reviews 2019.

[3] Li J, Liu Q, Duan Y, Yang Z. Performance analysis of organic Rankine cycles using R600/R601a mixtures with liquid-separated condensation. Applied Energy 2017; 190:376–89.

[4] Usman M, Imran M, Yang Y, Lee DH, Park B-S. Thermo-Economic Comparison of Air-Cooled and Cooling Tower Based Organic Rankine Cycle (ORC) with R245fa and R1233zde as Candidate Working Fluids for Different Geographical Climate Conditions. Energy 2017; 123:353–66.

[5] Wieland C, Kohlhepp A, Pili R, Eyerer S, Spliethoff H. Energy Conversion Method and System (EP 16 191 160.7, European Patent).

[6] García del Valle J, Sierra-Pallares J, Rodríguez Vega AS, Castro Ruiz F. Influence of the degree of superheating on the performance of a R134a condenser by means of experimental and numerical studies. International Journal of Refrigeration 2019; 98:25–34.

[7] Kwon OJ, Shon B, Kang YT. Experimental investigation on condensation heat transfer and pressure drop of a low GWP refrigerant R-1233zd(E) in a plate heat exchanger. International Journal of Heat and Mass Transfer 2019; 131:1009–21.

[8] Eyerer S, Dawo F, Kaindl J, Wieland C, Spliethoff H. Experimental Investigation of Modern ORC Working Fluids R1224yd(Z) and R1233zd(E) as Replacements for R245fa. Applied Energy 2019; 240:946-963.

[9] Lemmon EW, Huber ML, McLinden MO. REFPROP Reference Fluid Thermodynamic and Transport Properties: NIST Standard Reference Database 23, Version 10.0 2018.

[10] VDI-Gesellschaft Verfahrenstechnik und Chemieingenieurwesen (ed.). VDI-Wärmeatlas. 11th ed. Berlin: Springer Vieweg; 2013.

[11] Yan Y-Y, Lin T-F. Condensation heat transfer and pressure drop of refrigerant R-134a in a small pipe. International Journal of Heat and Mass Transfer 1999; 42(4):697–708.